Mathematical Biosciences 366 (2023) 109087

Contents lists available at ScienceDirect

Mathematical Biosciences

journal homepage: www.elsevier.com/locate/mbs

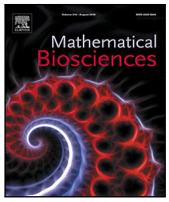

Original Research Article

Climate-dependent effectiveness of nonpharmaceutical interventions on COVID-19 mitigation

Juping Ji [a,b], Hao Wang [a,b,*], Lin Wang [c], Pouria Ramazi [d], Jude Dzevela Kong [e], James Watmough [c]

[a] Department of Mathematical and Statistical Sciences, University of Alberta, Edmonton, AB T6G 2R3, Canada
[b] Interdisciplinary Lab for Mathematical Ecology and Epidemiology, University of Alberta, Edmonton, AB T6G 2R3, Canada
[c] Department of Mathematics and Statistics, University of New Brunswick, Fredericton, NB E3B 5A3, Canada
[d] Department of Mathematics and Statistics, Brock University, St. Catharines, ON L2S 3A1, Canada
[e] Department of Mathematics and Statistics, York University, Toronto, ON M3J 1P3, Canada

ARTICLE INFO

MSC:
34D20
49M05
92B05

Keywords:
Transmission rate
Inverse method
Environmental conditions
Machine learning
Generalized boosting model
Nonpharmaceutical interventions

ABSTRACT

Environmental factors have a significant impact on the transmission of infectious diseases. Existing results show that the novel coronavirus can persist outside the host. We propose a susceptible–exposed–presymptomatic–infectious–asymptomatic–recovered–susceptible (SEPIARS) model with a vaccination compartment and indirect incidence to explore the effect of environmental conditions, temperature and humidity, on the transmission of the SARS-CoV-2 virus. Using climate data and daily confirmed cases data in two Canadian cities with different atmospheric conditions, we evaluate the mortality rates of the SARS-CoV-2 virus and further estimate the transmission rates by the inverse method, respectively. The numerical results show that high temperature or humidity can be helpful in mitigating the spread of COVID-19 during the warm summer months. Our findings verify that nonpharmaceutical interventions are less effective if the virus can persist for a long time on surfaces. Based on climate data, we can forecast the transmission rate and the infection cases up to four weeks in the future by a generalized boosting machine learning model.

1. Introduction

SARS-CoV-2 has caused a serious pandemic in the past three years and directly threatened global health systems. One current concern is the appearance of many SARS-CoV-2 variants, such as Alpha, Beta, Gamma, Delta and Omicron since 2019. These new variants spread more easily and quickly than the original viral strain. A tremendous amount of work on COVID-19 has been carried out in the past two years [1–7]. Nonpharmaceutical interventions (NPIs), policies from the government, are used to reduce the spread of some endemic, directly transmitted, respiratory infections diseases, which has been proven to be an effective strategy in reducing the transmission of COVID-19 [2,8–11].

COVID-19 is believed to be spread in several different ways. Evidence suggests the virus transmits mainly between people who are in close contact with infected individuals [12]. However, particles of different sizes (droplets and aerosols) containing virus can also spread indoors or in poorly ventilated areas [13–15]. In practice, contact with contaminated surfaces also plays an important role in the spread of COVID-19 [16–21]. Rwezaura et al. [21] showed that the virus in the environment has a significant effect on the transmission of COVID-19. The virus can be transmitted to uninfected individuals by contamination of nearby surfaces. In this situation, understanding the factors that contribute to the persistence of the virus on the environmental surface will be helpful to mitigate the risk of COVID-19 transmission.

Environmental factors such as temperature, humidity, precipitation, may play a significant role in the transmission of viruses [1,3,16,22–26]. McClymont and Hu [24] suggested that weather and climate can affect the transmission of COVID-19 significantly, and weather covariates (temperature and humidity) can facilitate the increase of COVID-19 transmission. Casanova et al. revealed that virus survival is enhanced by lower air temperature and relative humidity [22]. In 2020, Prata et al. [26] explored the relationship between annual average temperature and COVID-19 confirmed cases for all 27 state capital cities of Brazil. Their results explained that as temperature ranges from 16.8 °C to 27.4 °C, it has a negative linear relationship with the number of confirmed cases.

Environmental conditions can affect the stability of SARS-CoV-2. Matson et al. pointed out that the virus is more stable at low-temperature and low-humidity conditions in nasal mucus and sputum,

* Corresponding author.
E-mail address: hao8@ualberta.ca (H. Wang).

https://doi.org/10.1016/j.mbs.2023.109087
Received 7 January 2023; Received in revised form 9 October 2023; Accepted 12 October 2023
Available online 18 October 2023

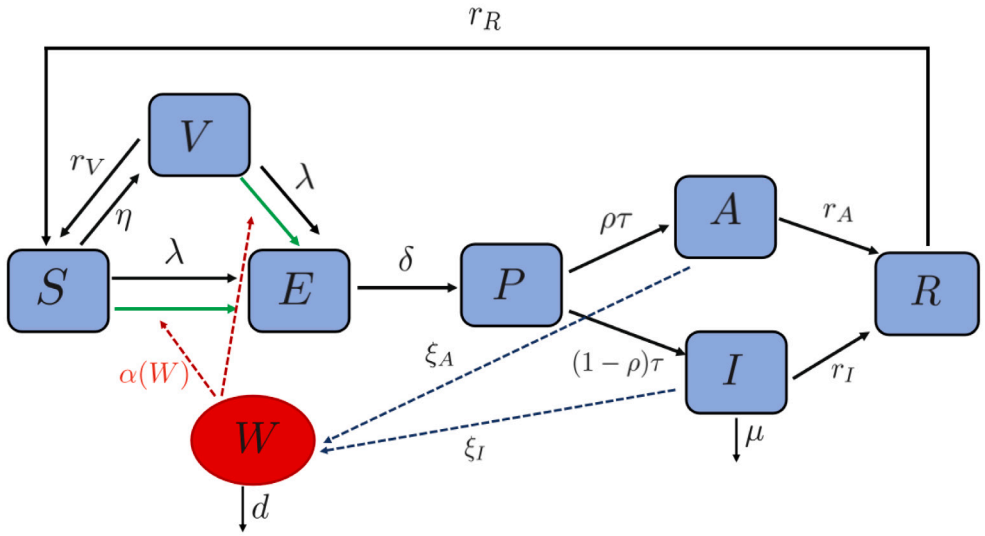

Fig. 1. Disease transmission flow of the System (2.1). We extended the susceptible–exposed–infectious–recovered model to include seven compartments: susceptible (S), exposed (E), presymptomatic infected (P), symptomatic infected (I), asymptomatic infected (A), recovered (R), and the vaccinated individuals (V). W denotes the density of SARS-CoV-2 on environmental surfaces. Black solid line denotes the status transition. Black dashed line represents the virus shedding from infected individuals. Red dashed line represents the indirect infection. Blue solid line denotes the status transition due to indirect infection.

Table 1
Half-life of SARS-CoV-2 exposed to different environmental conditions.
Source: Adapted from a slide shared by Bryan: https://www.washingtonpost.com/weather/2020/04/23/lab-study-coronavirus-summer-weather/.

Condition	Temperature	Humidity	Solar	Half life
Surface	70–75 °F	20%	None	18 h
Surface	70–75 °F	80%	None	6 h
Surface	95 °F	80%	None	1 h
Surface	70–75 °F	80%	Summer	2 min

warmer temperature and higher humidity may result in decreased virus transmission [23]. In 2020, Bryan studied the effect of sunlight, temperature and humidity on the half-life of the virus respectively in his laboratory experiment, and found that sunlight, higher temperature and humidity can decrease the stability of coronavirus at the daily press [27]. As shown in Table 1, temperature, humidity and sunlight are significant factors affecting the decay of SARS-CoV-2. In the absence of sunlight, at ambient indoor temperature, increasing humidity can reduce the half-life of coronavirus. At the same humidity conditions, higher temperature can shorten the half-life of the virus. Adding in sunlight, the half-life of coronavirus reduces accordingly at the same temperature and humidity conditions. This finding reveals that the coronavirus exposed to direct sunlight or warmer temperature or higher humidity would die quickly. In 2020, Biryukov et al. [28] showed that the half life ($t_{1/2}$) of SARS-CoV-2 on surfaces is determined by the function of temperature and relative humidity as follows:

$$t_{\frac{1}{2}} = 32.426272 - 0.622108T - 0.153707H,$$

where T denotes the temperature in degrees Celsius and H represents the percent relative humidity. The half-life of the virus is inversely proportional to increasing temperature and relative humidity. Similar to the flu, in colder months, the coronavirus survives longer and appears to spread efficiently [1,22,24,29].

2. Model formulation

Environmental surfaces are considered to be conducive to the spreading of the virus. Existing results show that the SARS-CoV-2 virus can persist outside the host [1,3]. Therefore, it is necessary to consider the transmission dynamics of SARS-CoV-2 on environmental surfaces. In our work, the transmission of SARS-CoV-2 is divided into two parts, direct transmission (contact from an infected person to another person without a contaminated intermediate object) and indirect transmission (contact with a contaminated intermediate object). Several studies have analyzed compartmental models describing human population and bacterial population, and explored the transmission dynamics [30–34].

Susceptible–exposed–infectious–recovered framework can well model the dynamics of COVID-19 transmission. With the implementation of the vaccination policy, we take the vaccination population into account. Then the total population size (N) is divided into seven compartments, the susceptible (S), the exposed (E), the presymptomatic infected (P), the symptomatic infected (I), the asymptomatic infected (A), the recovered individuals (R), and the vaccinated individuals (V), hence $N = S + E + P + I + A + R + V$. In this paper, we propose a susceptible–exposed–presymptomatic–infectious–asymptomatic–recovered–susceptible (SEPIARS) model with a vaccination compartment and indirect incidence:

$$\begin{cases} \frac{dS}{dt} = -\lambda S - \alpha(W)S - \eta S + r_V V + r_R R, \\ \frac{dE}{dt} = \lambda[S + (1-\sigma)V] + \alpha(W)[S + (1-\sigma)V] - \delta E, \\ \frac{dP}{dt} = \delta E - \tau P, \\ \frac{dI}{dt} = (1-\rho)\tau P - (\mu + r_I)I, \\ \frac{dA}{dt} = \rho\tau P - r_A A, \\ \frac{dR}{dt} = r_I I + r_A A - r_R R, \\ \frac{dV}{dt} = \eta S - \lambda(1-\sigma)V - \alpha(W)(1-\sigma)V - r_V V, \\ \frac{dW}{dt} = \xi_I I + \xi_A A - d(T,H)W \end{cases} \tag{2.1}$$

with nonnegative initial conditions $S(0)$, $E(0)$, $P(0)$, $I(0)$, $A(0)$, $R(0)$, $V(0)$, $W(0)$. Here λ is the force of infection and is defined as $\lambda = \frac{\beta(T,H)(I+\theta_A A+\theta_p P)}{N}$. W denotes the density of SARS-CoV-2 on environmental surfaces. A schematic diagram for System (2.1) is presented in Fig. 1. Here $\beta(T,H)$ represents the transmission parameter for direct transmission, which depends on temperature and humidity, here T denotes the temperature and H represents humidity. η is the vaccination rate. Various COVID-19 vaccines were at clinical development stage in 2021. Most people in Canada took the Pfizer and Moderna vaccines which have similar efficacy in 2021 [42], then we use σ to represent the

Table 2
The parameter description of System (2.1).

Parameter	Description	Unit	Value	Source
β	Transmission rate for direct transmission	day^{-1}		
θ_P	Relative transmissibility of presymptomatic individuals		0.55	[6,35]
θ_A	Relative transmissibility of asymptomatic infected individuals		0.55	[6,35]
η	Vaccination rate	day^{-1}	0–0.055	[36]
σ	Vaccine efficacy		0.8	Assumed
$1/\delta$	The mean length of latent period	day	2.9	[12,35]
$1/\tau$	The pre-symptomatic infectious period	day	2	[37]
ρ	Proportion of asymptomatic infected individuals		0.6	[35]
μ	Death rate of symptomatic infected individuals due to SARS-CoV-2	day^{-1}	0.0008–0.0016	[38,39]
r_I	Symptomatic infected individuals recovery rate	day^{-1}	1/11	[35]
r_A	Asymptomatic infected individuals recovery rate	day^{-1}	1/7	[35]
r_R	Rate at which recovered individuals lose immunities	day^{-1}	1/180–1/90	[40,41]
r_V	Rate at which vaccinated individuals lose immunities	day^{-1}	1/180–1/90	[40,41]
a	Maximum rate of infection	day^{-1}	0.0001	Assumed
b	Half-saturation of the virus density	cells	600 000	Assumed
ξ_I	Virus shedding rate from symptomatic infected individuals	cells ind^{-1} day^{-1}	13.5	[39]
ξ_A	Virus shedding rate from asymptomatic infected individuals	cells ind^{-1} day^{-1}	3.4	[39]
d	Mortality rate of SARS-CoV-2	day^{-1}		Estimated

vaccine efficacy ($0 \le \sigma \le 1$). If $\sigma = 1$, the vaccine offers 100% protection against the epidemic. Some studies suggest that COVID-19 vaccines are highly effective against SARS-CoV-2 after two doses, but the protection seems to be reduced over time [43–45]. Due to the incidence terms and the decline of vaccination protection, if the susceptible and vaccinated individuals are infected by presymptomatic (P), symptomatic (I) and asymptomatic infected individuals (A), they will all enter the exposed individuals (E). θ_P and θ_A are the relative transmissibility of presymptomatic and asymptomatic infected individuals, respectively. $1/\delta$ is the incubation period. r_I and r_A denote recovery rates of the symptomatic and asymptomatic infected individuals, respectively. Asymptomatic infections account for a proportion of ρ, and symptomatic infections account for a proportion of $1-\rho$. In this work, we assume that there are no births, as well as no deaths unrelated to COVID-19. μ is the virus-caused death rate of symptomatic infected individuals. Recovered and vaccinated individuals may lose immunities and be reinfected by SARS-CoV-2 [40,41,46]. Edridge et al. [40] showed that after a duration of six months, about 50% of recovered individuals start losing their antibodies. We use r_R and r_V to represent the rates at which recovered and vaccinated individuals lose immunities, separately. Since infected patients can generate SARS-CoV-2 by coughing, talking, and sneezing, we use ξ_I and ξ_A to represent the virus shedding rates of symptomatic and asymptomatic infected individuals, respectively. Here $d(T,H)$ denotes the death rate of SARS-CoV-2 on the environmental surface, which depends on temperature and humidity. $\alpha(W)$ is the indirect part of the incident term, which is defined by $\alpha(W) = \frac{aW}{W+b}$. The description of the parameters of System (2.1) is specified in Table 2.

The rest of this paper is organized as follows. We evaluate the mortality rates of SARS-CoV-2 in two Canadian cities with different environmental conditions and compare the dynamics of System (2.1) under different viral mortality rates in Section 3. In Section 4, we consider a time-dependent transmission rate and explore the effect of weather conditions on the transmission rate. The effect of NPIs on mitigating the transmission of COVID-19 under different atmospheric conditions is presented in Section 5. We employ a machine learning approach with climate data to make predictions of daily infection cases in Section 6. In Section 7, we discuss the assumptions and limitations of our study. We summarize and discuss our findings in the last section.

3. Evaluation of $d(T,H)$

To explore the impact of environmental conditions on the mortality rate of SARS-CoV-2 on surfaces, we choose two cities, Edmonton in Alberta and Vancouver in British Columbia, Canada, with distinct climatic conditions. We first collect the data of temperature and relative humidity in Edmonton and Vancouver from January 1 to December 31 in 2021 [47]. Fig. 2(a) presents the average temperature in Edmonton and Vancouver. From Fig. 2(a), we observe that the average temperature in Vancouver is obviously higher than in Edmonton in cold months. In the warm months (June, July, August, and September), the average temperatures in the two cities are close. The average relative humidity in two cities is described in Fig. 2(b). Fig. 2(b) shows that the relative humidity in Vancouver is higher than that in Edmonton in 2021.

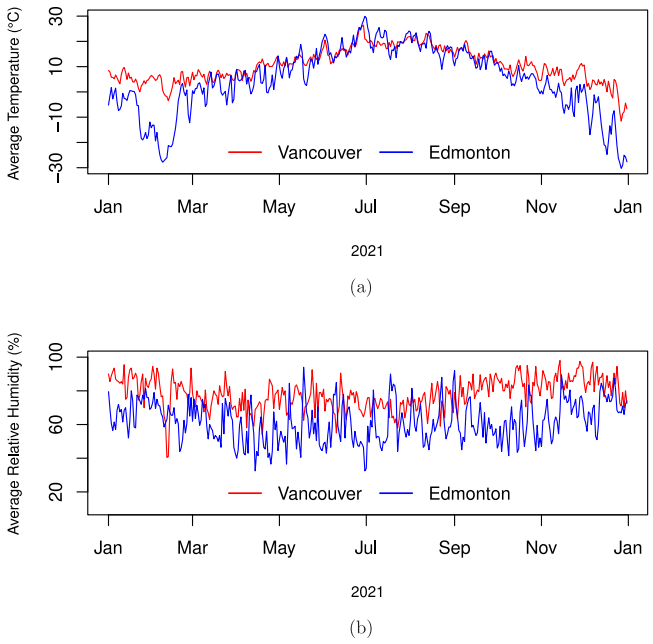

Fig. 2. Average temperature and relative humidity in Edmonton and Vancouver in 2021.

In 2020, Biryukov et al. [28] fitted a linear regression equation, which models the half-life of SARS-CoV-2 at the combination of temperature and relative humidity conditions. They estimated that the mean half life ($t_{1/2}$) of SARS-CoV-2 on surfaces is a function of temperature in degrees Celsius (T) and percent relative humidity (H) in hours:

$$t_{\frac{1}{2}} = 32.426272 - 0.622108T - 0.153707H.$$

Consider e^{-dt} is the surviving probability of the virus at time t. From the function of the half life ($t_{1/2}$) of SARS-CoV-2 on surfaces, with the relation $e^{-dt} = 0.5$, we can calculate the mortality rates of SARS-CoV-2

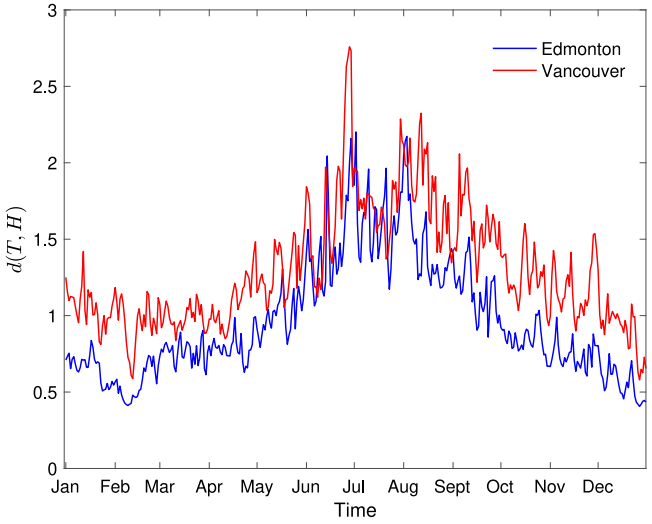

Fig. 3. Mortality rates of SARS-CoV-2 on surfaces in Edmonton and Vancouver.

under different weather conditions in days:

$$d(T,H)=\frac{\ln 2}{t_{\frac{1}{2}}}=\frac{\ln 2}{(32.426272-0.622108T-0.153707H)/24}.$$

Then we can substitute the daily temperature and relative humidity data into above function to obtain the corresponding daily mortality rate of SARS-CoV-2 in Edmonton and Vancouver, separately. As presented in Fig. 3, the mortality rate of SARS-CoV-2 on surfaces in Edmonton is lower than that in Vancouver. It should be pointed out that, beginning in March, with the increase of temperature in two cities, the mortality rates of SARS-CoV-2 on surfaces increase correspondingly, and the mortality rates both reach the maximum value in summer. High temperature and humidity can reduce the survival time of SARS-CoV-2, hence leading to a higher viral mortality rate. After September, since the average temperatures in Edmonton and Vancouver decrease, the mortality rates of the SARS-CoV-2 virus on surfaces also decrease.

4. A time varying transmission rate

In this section, we consider a time-dependent transmission rate $\beta(t)$ of System (2.1) to study the effect of environmental factors on the spread of COVID-19. To explore the time varying transmission rates in Edmonton and Vancouver in 2021, we collect the number of daily confirmed cases in these two cities from January 1 to December 31 [48]. The 7-day moving average is a useful tool to smooth out regular daily fluctuations. Given that the number of daily confirmed cases may be underreported or delayed during the weekend, motivated by the work in [49], we take the 7-day averaged confirmed cases (the average of the last 6 days and the current day) to reduce the inaccuracy of daily reported confirmed cases. As shown in Fig. 4(a), the daily confirmed cases in two cities in July are significantly lower than that in other months. The comparison presents the daily confirmed cases in Edmonton are higher than that in Vancouver.

Inverse method [49–53] is a useful tool to extract the time-dependent transmission rate from infection data. It is a well-known discrete method for estimating the time-varying transmission rate inversely. Using the data of daily confirmed cases in Edmonton and Vancouver in Canada, we intend to estimate the transmission rates in these two cities by the inverse method, respectively. Let $S[i]$, $E[i]$, $P[i]$, $I[i]$, $A[i]$, $R[i]$, $V[i]$ and $W[i]$ denote the values of variables in System (2.1) on day i. We choose $(1-\rho)\tau P(t)$ as the approximate value of the notification data and let $M[i]=(1-\rho)\tau P(t)$ represent the daily notification data on the ith day, then we have $P[i]=\frac{M[i]}{(1-\rho)\tau}$, $i=1,2,\dots,K$, where K denotes the length of the vector of the notification data. With the relation $N=S(t)+E(t)+P(t)+I(t)+A(t)+R(t)+V(t)$, we have $N=S[1]+E[1]+P[1]+I[1]+A[1]+R[1]+V[1]$. Initial value $I[1]$ is reported from the Website [48] and we assume that $A[1]=2I[1]$.

From the third equation of System (2.1), we can get

$$E[i]=\frac{P[i+1]+(\tau-1)P[i]}{\delta}.$$

Then from the second equation of System (2.1), we have

$$E[2]-E[1]=\frac{\beta[1](S[1]+(1-\sigma)V[1])(I[1]+\theta_P P[1]+\theta_A A[1])}{N}+\alpha(W[1])(S[1]+(1-\sigma)V[1])-\delta E[1].$$

Hence, we can obtain that

$$\beta[1]=\frac{[E[2]-E[1]+\delta E[1]-\alpha(W[1])(S[1]+(1-\sigma)V[1])]N}{(S[1]+(1-\sigma)V[1])(I[1]+\theta_P P[1]+\theta_A A[1])}.$$

Then from System (2.1), it follows that

$$I[i]=I[i-1]+(1-\rho)\tau P[i-1]-(r_I+\mu)I[i-1],$$

$$A[i]=A[i-1]+\rho\tau P[i-1]-r_A A[i-1],$$

$$R[i]=R[i-1]+r_I I[i-1]+r_A A[i-1],$$

$$W[i]=W[i-1]+\xi_I I[i-1]+\xi_A A[i-1]-d(T,H)W[i-1],$$

$$S[i]=S[i-1]-\frac{\beta[i-1]S[i-1](I[i-1]+\theta_P P[i-1]+\theta_A A[i-1])}{N}-\alpha(W[i-1])S[i-1]-\eta S[i-1]+r_V V[i-1]+r_R R[i-1],$$

$V[i]=N-S[i]-E[i]-P[i]-I[i]-A[i]-R[i]$, for $i=2,3,\dots,K$. Here

$$\beta[i]=\frac{[E[i+1]-E[i]+\delta E[i]-\alpha(W[i])(S[i]+(1-\sigma)V[i])]N}{(S[i]+(1-\sigma)V[i])(I[i]+\theta_P P[i]+\theta_A A[i])}$$

for $i=2,3,\dots,K-1$, and $\beta[K]\approx\beta[K-1]$.

From Statistics Canada [54], we obtain the total population of Edmonton and Vancouver are 1,418,118 and 2,642,825 in 2021, respectively. Here, we keep θ_A, θ_P, δ, ρ, r_I, r_A, ξ_I, and ξ_A at their baseline values. These are $\theta_A=\theta_P=0.55$ [6,35], $\delta=1/2.9$ [12,35], $\rho=0.6$ [35], $r_I=1/11$ [35], $r_A=1/7$ [35], $\xi_I=13.5$ [39], and $\xi_A=3.4$ [39]. Since presymptomatic individuals start transmitting the infection 1–2 days to the end of the incubation period, we take $\tau=1/2$. Previous studies have estimated μ between 0.0008 and 0.0016 [38,39]. We take μ to be on the low end of this range, since these studies are based on conditions outside of Canada, and we assume that Canada would have a lower death rate by world standards due to its relatively high quality of medical care. We take r_V to be 1/180, close to the low end of its estimated range [40,41], as the time window analyzed in this paper covers time in which most vaccinated individuals only had one dose (which would lead to faster waning of immunity). Furthermore, we take $r_R=1/180$ under the assumption that immunity conferred by recovery is same to the immunity due to vaccination. We assume a value of 0.8 for σ because available vaccines generally provided good levels of protection against the strains of SARS-CoV-2 present during 2021 (e.g. the original strain, Alpha, Delta). For η, we take a value of 0.004. Although the vaccination rate in Canada varied during 2021 [36], we find a rate of 0.4 percent of the population per day to be a reasonable average for 2021. a and b are fitted in order to ensure that the derived transmission rate was non-negative and not unreasonably large. Then, we use available data on climate and daily confirmed cases in Edmonton and Vancouver to obtain the transmission rate $\beta(t)$ separately. As shown in Fig. 4(b), transmission rates in two cities are obtained by the inverse method, respectively. Moreover, we observe that the daily confirmed cases and transmission rates in Edmonton and Vancouver in June and July are well lower than that in November and December. These numerical results verify that the transmission rate of COVID-19 is low in the warm summer months, while cold winter months can lead to high transmission rates.

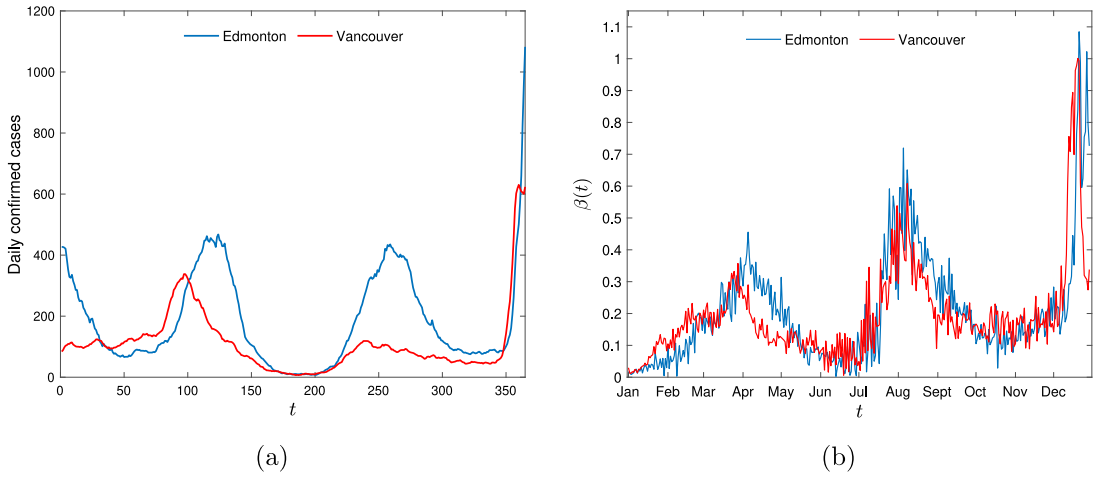

Fig. 4. (a) Daily confirmed cases in Edmonton and Vancouver in 2021. (b) Transmission rates in Edmonton and Vancouver obtained by the inverse method.

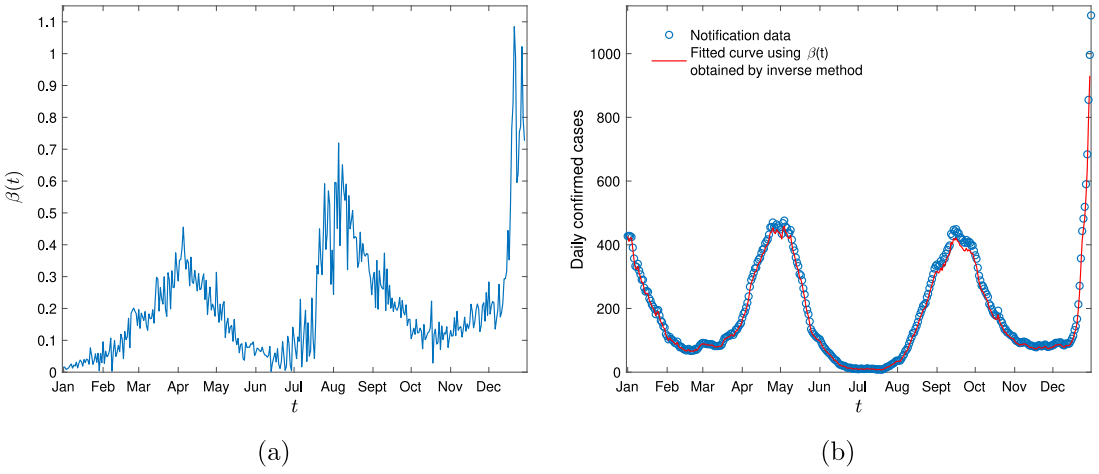

Fig. 5. Transmission rate in Edmonton obtained by the inverse method and the fitting with notification data. Initial condition is $(S[1], E[1], P[1], I[1], A[1], R[1], V[1], W[1]) = (1000000, 2847, 2135, 44800, 89600, 37444, 241292, 200000)$.

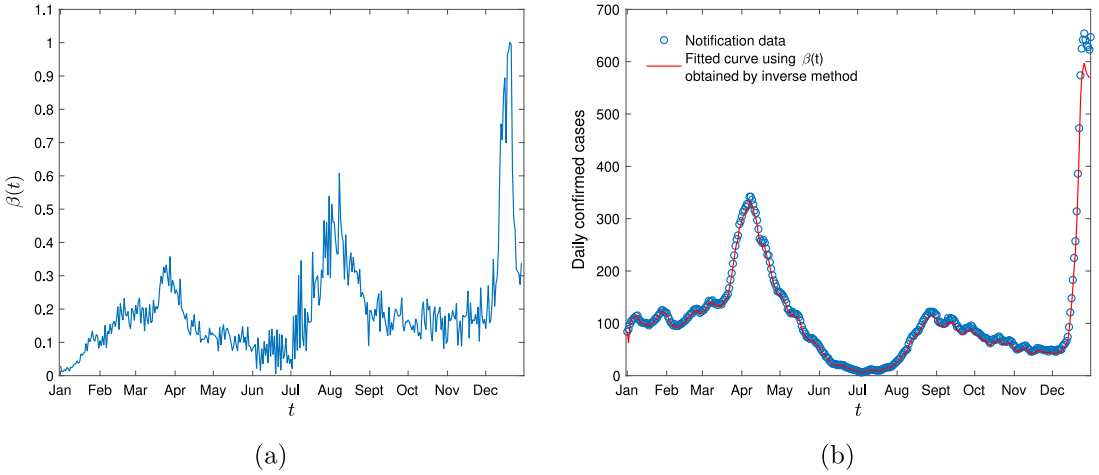

Fig. 6. Transmission rate in Vancouver obtained by the inverse method and the fitting with notification data. Initial condition is $(S[1], E[1], P[1], I[1], A[1], R[1], V[1], W[1]) = (2000000, 800, 420, 12373, 24746, 11000, 593486, 400000)$.

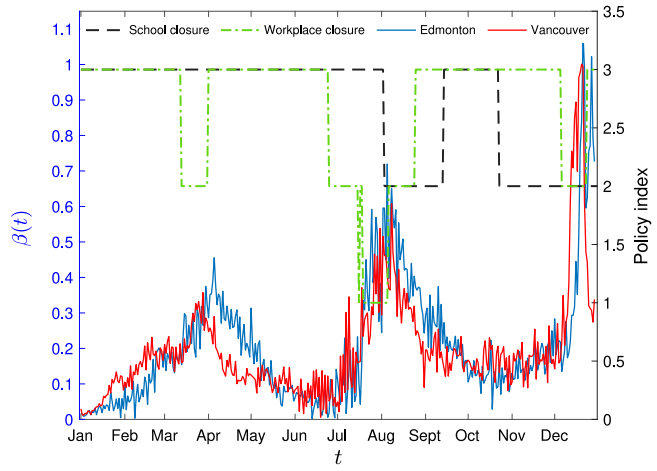

Fig. 7. Transmission rates in Edmonton and Vancouver and government policies on school and workplace closures in 2021.

Figs. 5(a) and 6(a) illustrate the transmission rate $\beta(t)$ extracted from daily confirmed cases data in Edmonton and Vancouver in 2021, respectively. Then we use the obtained transmission rates $\beta(t)$ to fit the daily notification data in Edmonton and Vancouver, respectively. We substitute the daily transmission rate $\beta(t)$ obtained by inverse method into System (2.1) to obtain $P(t)$, then plot the curve of $(1-\rho)\tau P(t)$ to compare with notification data. As presented in Figs. 5(b) and 6(b), we observe that both transmission rates obtained by the inverse method fit the notification data almost perfectly.

5. Implementation of NPIs

NPIs, such as facial coverings, physical distancing, school and workplace closures are widely used to reduce the spread of COVID-19. These government policies have been proven to be an effective strategy in mitigating the transmission of COVID-19 [2,8–11]. In this section, we intend to explore the effect of NPIs on mitigating the transmission of COVID-19 under different climatic conditions. We collect the policy responses to the coronavirus pandemic of the government of Canada in 2021. The policy indices are obtained from the official website Our World In Data [55]. The index ranges from 0 to 3, records the strictness of government policies in 2021, where 0 represents no restrictions and 3 represents maximum restrictions. In this work, we focus on the government policies on school and workplace closures and compare the effectiveness of NPIs under different environmental conditions.

As presented in Fig. 7, we find that the implementation of NPIs has a great effect on mitigating the transmission of SARS-CoV-2. It should be noted that stricter policies on school and workplace closures can lead to a decrease of transmission rates in two cities. However, we observe that under the same strict policy, the transmission rate in Edmonton decreases slower than that in Vancouver between April and June, mid-August and mid-October.

In Fig. 3, we see that the mortality rate of SARS-CoV-2 in Vancouver is greater than that in Edmonton. Since SARS-CoV-2 can persist for a long time on surfaces under low temperature and humidity conditions, our work suggests that NPIs (school and workplace closures) are relatively less effective in reducing the transmission of COVID-19 in Edmonton than that in Vancouver. This finding verifies that if SARS-CoV-2 can survive on the surface for a long time, NPIs are less effective in mitigating the transmission of COVID-19.

6. Machine learning and prediction

In this section, we will explore the relationship between the transmission rate and climatic factors. The gradient boosting machine (GBM) is a powerful machine learning algorithm in statistics. It is a popular machine-learning technique which makes the prediction work simpler [56,57]. We plan to employ GBM to estimate the transmission rate from the average temperature and relative humidity with the gbm package and the predict function in **R**.

We divide the data into two parts, training dataset and testing dataset, where the training dataset is utilized to calibrate the parameters, and the testing dataset is used to test the model performance in making predictions. In Fig. 7, we observe that NPIs are effective to mitigate the transmission of COVID-19 after September. Then we choose and fix the start date of training on January 1 and let the training duration increase from 232 days. As shown in Table 3, we train GBM for different training durations increasing from 232 days to 316 days by 7 days and test the models for 28 days following each training duration. The daily transmission rates obtained by the inverse method and climatic factors compose the training dataset. Based on the climatic factors provided during the test duration, the trained GBM will give a prediction for the transmission rate. Then, we can use the time series of trained and tested daily transmission rates to evaluate the daily infection cases, and plot the curve of $(1-\rho)\tau P(t)$ of System (2.1). After that, we compare the predicted infection cases with the notification data of confirmed cases.

Table 3
Training and testing durations.

Train length (days)	Train duration	Test duration
232	January 1 – August 20, 2021	August 21 – September 17, 2021
239	January 1 – August 27, 2021	August 28 – September 24, 2021
246	January 1 – September 3, 2021	September 4 – October 1, 2021
253	January 1 – September 10, 2021	September 11 – October 8, 2021
260	January 1 – September 17, 2021	September 18 – October 15, 2021
267	January 1 – September 24, 2021	September 25 – October 22, 2021
274	January 1 – October 1, 2021	October 2 – October 29, 2021
281	January 1 – October 8, 2021	October 9 – November 5, 2021
288	January 1 – October 15, 2021	October 16 – November 12, 2021
295	January 1 – October 22, 2021	October 23 – November 19, 2021
302	January 1 – October 29, 2021	October 30– November 26, 2021
309	January 1 – November 5, 2021	November 6 – December 3, 2021
316	January 1 – November 12, 2021	November 13 – December 10, 2021

Table 4
MAPE and MAE of the predicted infection cases and notification confirmed cases under different training durations.

Train length (days)	MAPE (%)	MAE
232	65.52	37
239	24.93	17
246	24.19	16
253	11.90	8
260	10.66	7
267	10.43	6
274	11.61	6
281	10.87	6
288	13.35	6
295	8.28	4
302	12.85	5
309	15.75	5
316	28.29	9

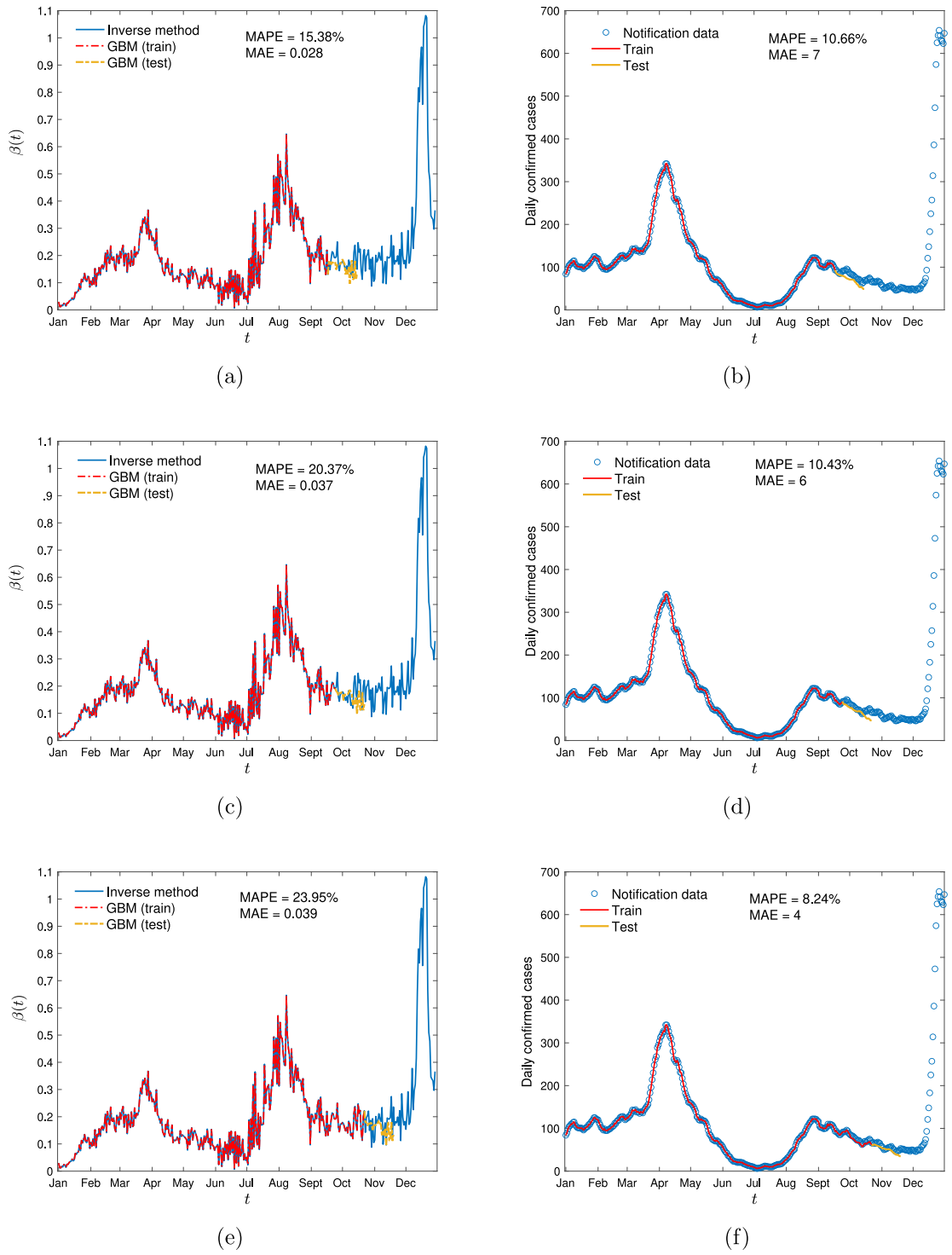

Fig. 8. (a)(b) Using climate data in Vancouver, train 260 days from January 1 to September 17, 2021, test 28 days from September 18 to October 15, 2021. (c)(d) Using climate data in Vancouver, train 267 days from January 1 to September 24, 2021, test 28 days from September 25 to October 22, 2021. (e)(f) Train 295 days from January 1 to October 22, 2021, test 28 days from October 23 to November 19, 2021.

In statistics, mean absolute percentage error (MAPE) is a common measure of prediction accuracy of a forecasting method, mean absolute error (MAE) is a measure of errors between paired observations expressing the same phenomenon [58,59]. In this work, we intend to use MAPE and MAE to evaluate the differences between the predicted infection cases and collected confirmed cases, and the differences between the transmission rates predicted by GBMs and those derived from the inverse method. Now, we introduce the formulas of MAPE and MAE:

$$\text{MAPE} = \frac{1}{n}\sum_{i=1}^{n}\left|\frac{y_i - x_i}{x_i}\right| \quad \text{and} \quad \text{MAE} = \frac{1}{n}\sum_{i=1}^{n}|y_i - x_i|$$

where x_i denotes the ith component of the vector of actual values, y_i is the ith component of the vector of prediction values, and n is the total number of data instances.

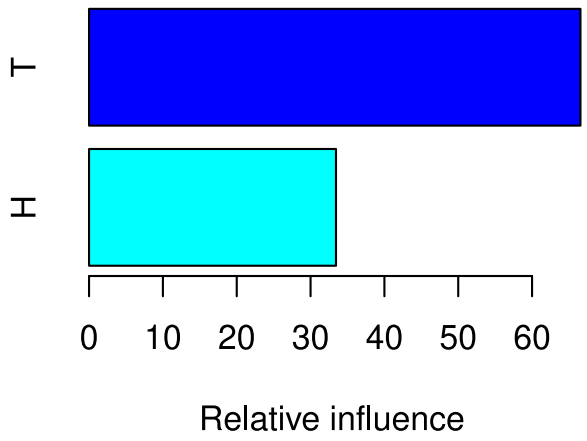

Fig. 9. Relative influence of temperature (T) and humidity (H) when trained for 295 days from January 1 to October 22, 2021.

We employ GBM with a learning rate of 0.01, 1000 trees with a Gaussian distribution of the response variable. The default depth of each tree is 30. A minimum number of 10 observations is allowed in the trees' terminal nodes and a 10 fold cross validation is performed. As we can see in Table 4, when the GBM is trained for 260 days, 267 days, and 295 days, small MAPEs and MAEs are obtained. As shown in Fig. 8, the prediction results based on each GBM are MAPE = 10.66%, MAPE = 10.43% and MAPE = 8.24%, separately. In Fig. 8, we observe that the trained transmission rates fit perfectly with the ones obtained from the inverse method. However, the predicted transmission rates do not fit well with the obtained transmission rate. Our numerical studies also exhibit that trained cases fit almost perfectly with the real notification confirmed data, and predicted infection cases fit quite well with the real data. Fig. 9 shows the relative influence of temperature and humidity in training the GBM. From Fig. 9, we see that temperature is the leading influential factor when the model is trained for 295 days.

7. Limitations

Our analysis has some limitations. The persistence of SARS-CoV-2 virus under environmental conditions is complex and may influenced by many factors, including temperature, humidity, surface type, and sunlight. In this paper, we only estimate the viral mortality rate at the combination of temperature and relative conditions, and explore the effects of temperature and relative humidity on the transmission of COVID-19. Another limitation is that we make assumptions of some parameters during the pandemic. Various COVID-19 vaccines are at clinical development stage, and these vaccines have different efficacy. However most people in Canada took the Pfizer and Moderna vaccines which have similar efficacy in 2021. We assume a high value for vaccine efficacy because available vaccines generally provided good levels of protection against the strains of SARS-CoV-2 present during 2021.

Data scarcity is a typical problem in our work. The notification data may underestimate the actual number of infections. 7-day moving average can be usually used to smooth out regular daily fluctuations and this method can contribute to prevent major events from distorting the data. In our work, to reduce the inaccuracy of daily reported confirmed cases, we use a 7-day moving average (the average of the last 6 days and the current day) to visualize the number of new COVID-19 cases in Edmonton and Vancouver. In addition, we assume vaccinated individuals have same immunity rates. Some individuals also get vaccinated even those who have already recovered from COVID-19. Since the vaccinated data of exposed, infected, and recovered individuals is not available, we do not introduce the vaccination in the recovered class in our simple compartmental model. This may lead to an underestimation of the vaccinated population. Then we may obtain low prediction results for the infection cases.

Our works verified that high temperature or humidity can be helpful in mitigating the spread of COVID-19 during the warm summer months numerically. To find the explicit expression for β as a function of T and H is an interesting but difficult work, which is beyond our analysis at this stage.

In this work, we focused on how environmental conditions affect the surface transmission. Existing works suggested that aerosol transmission is also an important mode for COVID-19 [60,61]. Understanding aerosol transmission will contribute to the control of the COVID-19 by reducing airborne transmission [62]. Environmental humidity can also affect the survival of pathogens in respiratory aerosols and droplets [63]. Exploring the effect of environmental conditions on aerosol transmission can promote us to understand the transmission mechanism of COVID-19.

8. Discussion

In this paper, we proposed an SEPIARS model with a vaccination compartment and indirect incidence. Using the climate data in two Canadian cities in 2021, we evaluated the mortality rates of the SARS-CoV-2 virus, respectively. We found that the mortality rate of the SARS-CoV-2 virus on environmental surfaces in Edmonton is lower than that in Vancouver. Then by analyzing daily confirmed cases and weather data in two cities, we extracted the time-varying transmission rates by inverse method, respectively. Moreover, we observed that the transmission rates obtained by the inverse method both give almost perfect fits with the notification data. Our results suggested that high temperature and humidity in the summers help reduce the spread potential of COVID-19, which verifies that environmental factors affect the transmission of COVID-19 [22,23,26]. The increased number of reported cases in the United States contradicts our findings. It is possible that some factors such as human behavior have exceeded the influence of weather conditions. However, in most countries, the available data enable us to better explore the effect of environmental factors on the number of confirmed cases, and their results also support that high temperature and high humidity mitigate the spread of COVID-19. These results indicated that the spread of COVID-19 might be seasonally associated with winter. It might be easier to control the spread of COVID-19 in the summer warm months.

In our work, we also studied the effect of NPIs on mitigating the transmission of COVID-19 under different atmospheric conditions. By comparing the effect of school and workplace closures on the spread of the SARS-CoV-2 virus in two cities with distinct climatic conditions, we found that if the virus can survive on the surface for a long time, NPIs are less effective in mitigating the COVID-19 epidemic. It is necessary to employ NPIs to help control the spread of COVID-19. The implementation of NPIs may lower the risk of coming in contact with SARS-CoV-2 on environmental surfaces. Hence, the transmission of COVID-19 can be decreased, and the burden of the epidemic on the healthcare system can be reduced as well.

To explore the relationship between the transmission rate and climatic factors, we employed gradient boosting machine to estimate the transmission rate from the climate data of Vancouver, and made predictions of the number of daily infection cases. We used MAE and MAPE to evaluate the prediction performance of the GBMs on the transmission rate and the fitting result of the number of confirmed cases. Our model shows perfect data fittings. Based on climate data, our model can be used to forecast the transmission rate and the infection cases up to four weeks in the future.

In addition to COVID-19, other human infectious diseases, such as cholera, malaria and dengue are all climate sensitive [64–67]. Climate variation drives the dynamics of cholera, malaria and dengue. In this paper, we only explored the impact of temperature and humidity on the

transmission of SARS-CoV-2. Besides these two factors, precipitation also plays an important role in the transmission of dengue, malaria and cholera disease. Modeling the climatic conditions can be helpful in making preparations for the outbreaks of these infectious diseases. Different from SARS-CoV-2, we need to consider the vectors of dengue, malaria and cholera viruses, such as water and mosquitoes. To apply our work to the study of the above climate-sensitive infectious diseases, it may be necessary to modify the infection mechanisms and incorporate more climatic factors. The methods in this paper can be used to make seasonal forecasts. In the future, we will continue to explore the impact of atmospheric conditions on the transmission of human infectious diseases, and try to use the inverse method and machine learning approaches to make predictions on the spread of climatic-sensitive infectious diseases.

CRediT authorship contribution statement

Juping Ji: Conceptualization, Methodology, Formal analysis, Visualization, Writing – original draft. **Hao Wang:** Conceptualization, Methodology, Writing – review & editing, Supervision, Funding acquisition. **Lin Wang:** Conceptualization, Methodology. **Pouria Ramazi:** Software. **Jude Dzevela Kong:** Methodology. **James Watmough:** Conceptualization, Methodology.

Declaration of competing interest

The authors declare that they have no conflict of interest concerning the publication of this manuscript.

Data availability

The datasets used and/or analyzed during the current study are available publicly [27,36,47,48,54,55].

Funding

This project is primarily supported by OMNI (One Health Modelling Network for Emerging Infections) funded by NSERC Emerging Infectious Diseases Modelling Initiative, Canada. JJ is supported by OMNI grant, HW's NSERC Discovery Accelerator Supplement Award, and departmental IUSEP funding. HW's research is partially supported by NSERC Individual Discovery, Canada Grant RGPIN-2020-03911 and Discovery Accelerator Supplement Award RGPAS-2020-00090. LW's research is partially supported by NSERC Individual Discovery, Canada Grant RGPIN-2020-04143.

References

[1] H.A. Aboubakr, T.A. Sharafeldin, S.M. Goyal, Stability of SARS-CoV-2 and other coronaviruses in the environment and on common touch surfaces and the influence of climatic conditions: A review, Transbound. Emerg. Dis. 68 (2021) 296–312.
[2] R.E. Baker, S.W. Park, W. Yang, et al., The impact of COVID-19 nonpharmaceutical interventions on the future dynamics of endemic infections, Proc. Natl. Acad. Sci. 117 (2020) 30547–30553.
[3] N.V. Doremalen, T. Bushmaker, D. Morris, M. Holbrook, et al., Aerosol and surface stability of SARS-CoV-2 as compared with SARS-CoV-1, New Engl. J. Med. 382 (2020) 1564–1567.
[4] X. Hao, S. Cheng, D. Wu, T. Wu, X. Lin, C. Wang, Reconstruction of the full transmission dynamics of COVID-19 in Wuhan, Nature 584 (2020) 420–424.
[5] R. Hirose, Y. Itoh, H. Ikegaya, et al., Differences in environmental stability among SARS-CoV-2 variants of concern: Both omicron BA.1 and BA.2 have higher stability, Clin. Microbiol. Infect. 28 (2022) 1486–1491.
[6] R. Li, S. Pei, B. Chen, Y. Song, T. Zhang, W. Yang, et al., Substantial undocumented infection facilitates the rapid dissemination of novel coronavirus(SARS-CoV-2), Science 368 (2020) 489–493.
[7] B.F. Maier, D. Brockmann, Effective containment explains subexponential growth in recent confirmed COVID-19 cases in China, Science 368 (2020) 742–746.
[8] M. Chinazzi, et al., The effect of travel restrictions on the spread of the 2019 novel coronavirus (COVID-19) outbreak, Science 368 (2020) 395–400.
[9] S. Hsiang, et al., The effect of large-scale anti-contagion policies on the COVID-19 pandemic, Nature 584 (2020) 262–267.
[10] S. Lai, et al., Effect of non-pharmaceutical interventions to contain COVID-19 in China, Nature 585 (2020) 410–413.
[11] L. Xue, S. Jing, H. Wang, Evaluating the impacts of non-pharmaceutical interventions on the transmission dynamics of COVID-19 in Canada based on mobile network, PLoS One 16 (12) (2021) e0261424.
[12] Q. Li, X. Guan, P. Wu, X. Wang, L. Zhou, Y. Tong, et al., Early transmission dynamics in Wuhan, China, of novel coronavirus-infected pneumonia, New Engl. J. Med. 382 (2020) 1199–1207.
[13] A. Fortin, M. Veillette, A. Larrotta, et al., Detection of viable SARS-CoV-2 in retrospective analysis of aerosol samples collected from hospital rooms of patients with COVID-19, Clin. Microbiol. Infect. 29 (2023) 805–807.
[14] M.C. Jarvis, Aerosol transmission of SARS-CoV-2: Physical principles and implications, Front. Public Health 8 (2020) 590041.
[15] A.A. Rabaan, S.H. Al-Ahmed, et al., Airborne transmission of SARS-CoV-2 is the dominant route of transmission: droplets and aerosols, Le Infezioni Med. 29 (1) (2021) 10–19.
[16] F. Carraturo, C. Del Giudice, M. Morelli, et al., Persistence of SARS-CoV-2 in the environment and COVID-19 transmission risk from environmental matrices and surfaces, Environ. Pollut. 265 (2020) 115010.
[17] P.Y. Chia, K.K. Coleman, Y.K. Tan, et al., Detection of air and surface contamination by SARS-CoV-2 in hospital rooms of infected patients, Nature Commun. 11 (2020) 2800.
[18] G. Correia, L. Rodrigues, M. Afonso, et al., SARS-CoV-2 air and surface contamination in residential settings, Sci. Rep. 12 (2022) 18058.
[19] S. Mwalili, M. Kimathi, V. Ojiambo, D. Gathungu, R. Mbogo, SEIR model for COVID-19 dynamics incorporating the environment and social distancing, BMC Res. Notes 13 (2020) 352.
[20] S.W.X. Ong, Y.K. Tan, P.Y. Chia, et al., Air, surface environmental, and personal protective equipment contamination by severe acute respiratory syndrome coronavirus 2(SARS-CoV-2) from a symptomatic patient, JAMA Netw. 323 (2020) 1610–1612.
[21] H. Rwezaura, S.Y. Tchoumi, J.M. Tchuenche, Impact of environmental transmission and contact rates on Covid-19 dynamics: A simulation study, Inform. Med. Unlocked 27 (2021) 100807.
[22] L.M. Casanova, S. Jeon, W.A. Rutala, D.J. Weber, M.D. Sobsey, Effects of air temperature and relative humidity on coronavirus survival on surfaces, Appl. Environ. Microbiol. 76 (2010) 2712–2717.
[23] M. Matson, C. Yinda, S.N. Seifert, T. Bushmaker, et al., Effect of environmental conditions on SARS-CoV-2 stability in human nasal mucus and sputum, Emerg. Infect. Diseases 26 (2020) 2276–2278.
[24] H. McClymont, W. Hu, Weather variability and COVID-19 transmission: A review of recent research, Int. J. Environ. Res. Public Health 18 (2021) 396.
[25] N. Pica, N.M. Bouvier, Environmental factors affecting the transmission of respiratory viruses, Curr. Opin. Virol. 2 (2012) 90–95.
[26] D.N. Prata, W. Rodrigues, P.H. Bermejo, Temperature significantly changes COVID-19 transmission in (sub)tropical cities of Brazil, Sci. Total Environ. 729 (2020) 138862.
[27] The washington post. Available from https://www.washingtonpost.com/weather/2020/04/23/lab-study-coronavirus-summer-weather/.
[28] J. Biryukov, J.A. Boydston, R.A. Dunning, J.J. Yeager, et al., Increasing temperature and relative humidity accelerates inactivation of SARS-CoV-2 on surfaces, mSphere 5 (2020) e00441–20.
[29] G.L. Nichols, E.L. Gillingham, H.L. Macintyre, et al., Coronavirus seasonality, respiratory infections and weather, BMC Infect. Dis. 21 (2021) 1101.
[30] A.A. Habees, E. Aldabbas, N.L. Bragazzi, J.D. Kong, Bacteria-bacteriophage cycles facilitate cholera outbreak cycles: An indirect Susceptible-Infected Bacteria-Phage (iSIBP) model-based mathematical study, J. Biol. Dyn. 16 (2022) 29–43.
[31] R.I. Joh, H. Wang, H. Weiss, J.S. Weitz, Dynamics of indirectly transmitted infectious diseases with immunological threshold, Bull. Math. Biol. 71 (2009) 845–862.
[32] J.D. Kong, W. Davis, H. Wang, Dynamics of a cholera transmission model with immunological threshold and natural phage control in reservoir, Bull. Math. Biol. 76 (2014) 2025–2051.
[33] J.H. Tien, D.J.D. Earn, Multiple transmission pathways and disease dynamics in a waterborne pathogen model, Bull. Math. Biol. 72 (2010) 1506–1533.
[34] A.R. Tuite, D.N. Fisman, A.L. Greer, Mathematical modelling of COVID-19 transmission and mitigation strategies in the population of Ontario, Canada, Can. Med. Assoc. J. 192 (2020) E497–E505.
[35] S. Jing, R. Milne, H. Wang, L. Xue, Vaccine hesitancy promotes emergence of new SARS-CoV-2 variants, J. Theoret. Biol. 570 (2023) 111522.
[36] Daily COVID-19 vaccine doses. Available from https://ourworldindata.org/covid-vaccinations.
[37] A. Rădulescu, C. Williams, K. Cavanagh, Management strategies in a SEIR–type model of COVID 19 community spread, Sci. Rep. 10 (2020) 21256.
[38] N.M. Ferguson, D. Laydon, G. Nedjati-Gilani, et al., Impact of non-pharmaceutical interventions (npis) to reduce covid-19 mortality and healthcare demand, in: Imperial College COVID-19 Response Team, 2020, p. 77482.

[39] L.M. Gomez, V.A. Meszaros, W.C. Turner, C.B. Ogbunugafor, The epidemiological signature of pathogen populations that vary in the relationship between free-living parasite survival and virulence, Viruses 12 (2020) 1055.
[40] A.W.D. Edridge, J. Kaczorowska, A.C.R. Hoste, et al., Seasonal coronavirus protective immunity is short-lasting, Nat. Med. 26 (2020) 1691–1693.
[41] I.M. Wangari, S. Sewe, et al., Mathematical modelling of COVID-19 transmission in Kenya: a model with reinfection transmission mechanism, Comput. Math. Methods Med. 2021 (2021) 1–18.
[42] P. Olliaro, E. Torreele, M. Vaillant, COVID-19 vaccine efficacy and effectiveness-the elephant (not) in the room, Lancet Microbe 2 (2021) E279–E280.
[43] J.I. Cohen, P.D. Burbelo, Reinfection with SARS-CoV-2: implications for vaccines, Clin. Infect. Dis. 73 (2021) e4223–e4228.
[44] S.Y. Tartof, J.M. Slezak, et al., Durability of BNT162b2 vaccine against hospital and emergency department admissions due to the omicron and delta variants in a large health system in the USA: a test-negative case–control study, Lancet Respir. Med. 10 (2022) 689–699.
[45] S.Y. Tartof, J.M. Slezak, et al., Effectiveness and durability of BNT162b2 vaccine against hospital and emergency department admissions due to SARS-CoV-2 omicron sub-lineages BA.1 and BA.2 in a large health system in the USA: a test-negative, case-control study, Lancet Respir. Med. 11 (2023) 176–187.
[46] J.L. Suah, M. Husin, et al., Waning COVID-19 vaccine effectiveness for BNT162b2 and CoronaVac in Malaysia: An observational study, Int. J. Infect. Dis. 119 (2022) 69–76.
[47] Weather dashboard for Canada. Available from https://www.weatherstats.ca/.
[48] Daily confirmed cases in Edmonton and Vancouver. Available from https://data.edmonton.ca/Community-Services/COVID-19-in-Edmonton-Daily-Active-Cases/qkyj-dqjp and http://www.bccdc.ca/health-info/diseases-conditions/covid-19/data.
[49] X. Wang, H. Wang, P. Ramazi, K. Nah, M. Lewis, From policy to prediction: Forecasting COVID-19 dynamics under imperfect vaccination, Bull. Math. Biol. 84 (9) (2022) 90.
[50] J.D. Kong, C. Jin, H. Wang, The inverse method for a childhood infectious disease model with its application to pre-vaccination and post-vaccination measles data, Bull. Math. Biol. 77 (2015) 2231–2263.
[51] A. Mummert, Studying the recovery procedure for the time-dependent transmission rate(s) in epidemic models, J. Math. Biol. 67 (2013) 483–507.
[52] M. Pollicott, H. Wang, H.H. Weiss, Extracting the time-dependent transmission rate from infection data via solution of an inverse ODE problem, J. Biol. Dyn. 6 (2012) 509–523.
[53] X. Wang, H. Wang, P. Ramazi, K. Nah, M. Lewis, A hypothesis-free bridging of disease dynamics and non-pharmaceutical policies, Bull. Math. Biol. 84 (5) (2022) 57.
[54] Statistics Canada. Available from https://www12.statcan.gc.ca/.
[55] Government policies on school and workplace closures. Available from https://ourworldindata.org/coronavirus.
[56] J.H. Friedman, Greedy function approximation: a gradient boosting machine, Ann. Statist. 29 (2001) 1189–1232.
[57] A. Natekin, A. Knoll, Gradient boosting machines, a tutorial, Front. Neurorobotics 7 (2013).
[58] U. Khair, H. Fahmi, S. Hakim, R. Rahim, Forecasting error calculation with mean absolute deviation and mean absolute percentage error, J. Phys. Conf. Ser. 930 (2017) 012002.
[59] C.J. Willmott, K. Matsuura, Advantages of the mean absolute error (MAE) over the root mean square error (RMSE) in assessing average model performance, Clim. Res. 30 (2005) 79–82.
[60] J.W. Tang, L.C. Marr, Y. Li, I. Eames, The role of SARS-CoV-2 aerosol transmission during the COVID-19 pandemic, Interface Focus 12 (2022) 20220003.
[61] R. Tellier, COVID-19: the case for aerosol transmission, Interface Focus 12 (2022) 20210072.
[62] C.C. Wang, K.A. Prather, J. Sznitman, et al., Airborne transmission of respiratory viruses, Science 373 (6558) (2021) eabd9149.
[63] E. Huynh, A. Olinger, D. Woolley, et al., Evidence for a semisolid phase state of aerosols and droplets relevant to the airborne and surface survival of pathogens, Proc. Natl. Acad. Sci. 119 (4) (2022) e2109750119.
[64] Z. Asadgol, H. Mohammadi, M. Kermani, A. Badirzadeh, M. Gholami, The effect of climate change on cholera disease: The road ahead using artificial neural network, PLoS ONE 14 (11) (2019) e0224813.
[65] C. Caminade, S. Kovats, J. Rocklov, et al., Impact of climate change on global malaria distribution, Proc. Natl. Acad. Sci. 111 (9) (2014) 3286–3291.
[66] G. Constantin de Magny, R.R. Colwell, Cholera and climate: a demonstrated relationship, Trans. Am. Clin. Climatol. Assoc. 120 (2009) 119–128.
[67] L. Xu, L.C. Stige, et al., Climate variation drives dengue dynamics, Proc. Natl. Acad. Sci. 114 (1) (2016) 113–118.